Robotics and Autonomous Systems 122 (2019) 103310

Contents lists available at ScienceDirect

Robotics and Autonomous Systems

journal homepage: www.elsevier.com/locate/robot

An autonomous mobile robot with passive wheels propelled by a single motor

Satoshi Ito [a,*], Kosuke Niwa [b], Shoya Sugiura [c], Ryosuke Morita [a]

[a] Faculty of Engineering, Gifu University, Japan
[b] Graduate School of Engineering, Gifu University, Japan
[c] Graduate School of Natural Science and Technology, Gifu University, Japan

ARTICLE INFO

Article history:
Received 3 January 2019
Received in revised form 10 July 2019
Accepted 27 September 2019
Available online 1 October 2019

Keywords:
Wheeled mobile robot
Mechanism design
Single motor actuation
Autonomous propulsion
Motion control

ABSTRACT

This paper proposes a new propulsion mechanism for a passive-wheeled robot. By applying the propulsion principle of a two-wheeled skateboard, or "snakeboard," a mobile robot with a rotor is constructed. Although the robot moves based on the counter force of the rotor rotation, the timely alternation of the orientations of the front and rear wheels is required. The mechanism proposed herein drives the rotor and the wheel orientations simultaneously using a single motor. Simulation analyses based on a dynamical model confirmed the desired temporal relation in motion between the rotor and wheel orientation, and evaluated the effect of some mechanical parameters to the traveling distance of the robot. Some experiments conducted using the robot demonstrated not only straight-line propulsion, as expected, but also controlled curved motion. Finally, by providing feedback of the positional information, the robot was able to autonomously arrive at a goal position by driving itself with its single motor.

1. Introduction

Mobility greatly enhances the abilities of a robot. It not only enlarges the workspace of the robot but also enables tasks such as drone delivery or the exploration of dangerous locations. Paved areas are very commonplace, given that modern society is dependent on vehicles. On such a flat surface, wheeled systems provide an effective means of enhancing mobility. Even if the wheels are not driven, and instead are only attached as passive wheels, like those of a roller-skate or dolly, their presence enables easy movement over a flat surface, making it easier to move objects quickly, as in the case of our moving luggage without having to lift it. That is, one of the simplest means of providing a robot with mobility while saving energy and increasing the speed of motion would be fitting of passive wheels to the robot and providing an appropriate propulsion force.

Passive-wheel systems have been the subject of many studies. A so-called "snakeboard" is a good example of a non-holonomic system [1–8]. A more practical robot with passive wheels is a snake-type robot in which linked passive wheels are attached serially via active joints [9,10]. Some studies have set out to realize the autonomous maneuvering of toy vehicles, like the Roller Racer [11,12] or Trikke [13]. Legged robots equipped with passive wheels at their leg tips have been found to be capable of moving efficiently [14,15].

In a passive-wheeled system, the provision of the propulsion force is the most significant problem. The propulsion force has to be provided by the elaborate combined movement of mechanisms to which the passive wheels are attached. It would be advantageous if such movement could be produced from motion with a smaller degree of freedom (DoF), i.e., from the minimum possible number of motors.

In fact, within a robot, the motors are some of the heaviest, and most failure-prone because of the wear incurred in generating motion, of all mechanical parts. Therefore, reducing the number of motors should realize the benefits of easy acceleration/deceleration because of the small mass while minimizing the number of breakdowns by reducing the number of failure-prone parts. Given these advantages, the present study set out to achieve a passive-wheeled robot with a single motor. As its propulsion mechanism, the use of steering manipulation, like that seen with a "Roller Racer", was deemed possible. However, considering the speed of movement that is possible based on dynamic actions, we limited our study to a two-wheeled skateboard. In our opinion, the propulsion mechanism of a two-wheeled skateboard is basically the same as that of a snakeboard [16].

Many papers have reported on the control of the snakeboard. The driving, rotating and parking gaits were generated by defining the sinusoidal inputs with the different frequency ratios for the rotor and the wheel angle [1]. Bullo and Lewis showed that

* Corresponding author.
E-mail address: satoshi@gifu-u.ac.jp (S. Ito).

https://doi.org/10.1016/j.robot.2019.103310
0921-8890/

the snakeboard dynamics can be decoupled to two kinematically-controllable vector field, and provided a algorithm to settle it to the desired rest position by applying the basic motion primitives [2]. The paths of the board were calculated under the constant wheel angles and then the trajectory to the goal position was generated by combining them [3]. The passive-velocity field control is applied after decoupling vector field defined from the snakeboard dynamics [4]. A method where the motion of the rotor and the wheel angles are computed from the planned trajectory directing to the end position by introducing the momentum dynamics derived from the constraints, is proposed and extended [5–8]. Although the arrival to the goal position is realized theoretically or using simulations in these works, the achievement with the real robot is still difficult due to the hardness of the parameter identification as well as the effect of the friction sometimes neglected in its mathematical modelings. Another reason for the difficulty in achievement by robots is that most of these studies treats the motion planning where the motion of the rotor or the wheel angle are controlled in a feedforward manner. As the human skateboard motion, the rider often confirms their own position relative to the goal position, and adjust their own motion to control the board to reach there. Thus, this paper aims at reaching the goal position based on the feedback information of the position and orientations. In our opinion, utilizing the feedback information is realistic to achieve the robot control in the actual world to reduce the effect of the parameter uncertainties or un-modeled frictions.

From structural approach of the robot, on the other hand, Wang et al. [17] reported on the kinematic relationship between this roll rotation of the board body and the orientation of the front and rear wheels. In other studies, the motion planning required to attain a goal position [18] or the actual degree of propulsion that could be achieved by the robot [19] was studied. However, to the best of the authors' knowledge, no studies other than our previous works [20,21] have reported on a robot with a single motor that is capable of moving like a snakeboard. Actually, in our previous works [20,21], single-motor propulsion was achieved by constructing a mechanism with stoppers and torque limiters. However, the torque limiter was key to the design and, being a special device, was difficult to design and manufacture by ourselves. Thus, we here propose a new mechanism without any special mechanical parts. After analyzing the behavior of the proposed propulsion mechanism by computer simulations, we conduct some experimental researches using the robot we constructed to investigate its dynamical characteristics, and finally make it to reach the goal with the single-motor actuation.

2. Mechanical structure

2.1. Principle of propulsion

The propulsion mechanism adopted for the present study was inspired by the two-wheeled skateboard shown in Fig. 1. This board consists of two plates, one at the front and another at the back, which are connected by a joint containing a torsion spring. One passive wheel, i.e., a caster, is attached on the underside of each plate. The connecting joint can twist, which gives rise to deviations in the wheel orientation given that their axes are leant backward.

When a rider uses this type of board, he or she places a foot on each plate. Using his or her own weight, they twist the board to change the orientations of the wheels, e.g., the front wheel to the left and the rear wheel to the right. Next, while maintaining this wheel orientation, they drive the board forward by turning the upper part of their body around their waist. This driving force propels the board and rider forward. Then, the rider recovers

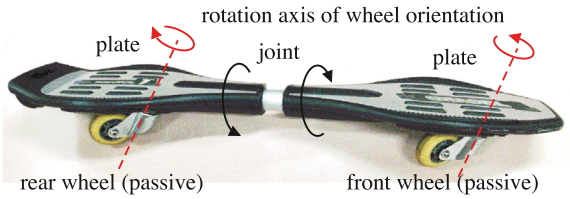

Fig. 1. Two-wheeled skateboard.

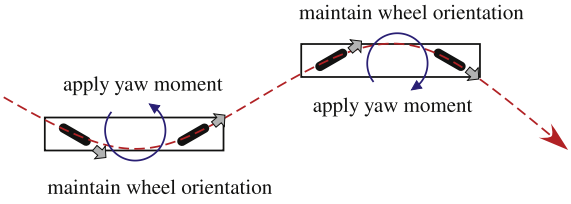

Fig. 2. Propulsion of the two-wheeled skateboard (snakeboard).

the board from the twisted state and then performs the same action but in the opposite direction. By repeating these actions, alternating from the left to the right, the rider makes the board travel forward with lateral undulation.

The essence of this propulsion principle is summarized in Fig. 2. The wheel orientation is symmetrical at the front and rear prior to the application of the yaw moment. Propulsion is achieved by the alternating side-to-side repetition of this operation.

2.2. Problems associated with single-motor actuation

This study set out to realize the propulsion mentioned in the previous section using only a single motor.

The means of propulsion would appear to be the same as that of a snakeboard. In the case of a snakeboard robot, however, three motors are usually utilized. One motor actuates a rotor to produce the yaw moment (corresponding to the turning of the upper body), and the other two motors each change the orientation of one of the wheels.

We regard these three types of actuation as being indispensable to the realization of propulsion. This implies that a rotor is essential to our design. However, it would appear difficult for us to simply connect them: the motor for the rotor is expected to generate the yaw moment, which requires acceleration. That is, dynamic motion is required. The other two motors, on the other hand, must change the wheel orientation and keep it constant to restrict the movement while the rotor is accelerating. That is, static regulation is required.

Thus, central to the problem of attaining single-motor actuation is how to simultaneously achieve these opposing dynamic and static requirements.

2.3. Proposed solution

Among the three actuations, the two responsible for changing the wheel orientations would appear to be easy to couple: the two wheels are usually positioned at the same height, and thus, two rotations can be attained within the same horizontal plane. Although the deviations of the front and rear wheel orientations could be different, we decided to make them equal by configuring the coupling accordingly. When the front wheel turns through θ_w to the left, the rear wheel turns through θ_w to the right. This symmetrical coupling is easy to realize using two gears of the same diameter.

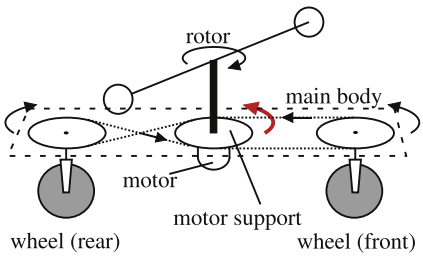

(a) Motor support and its function

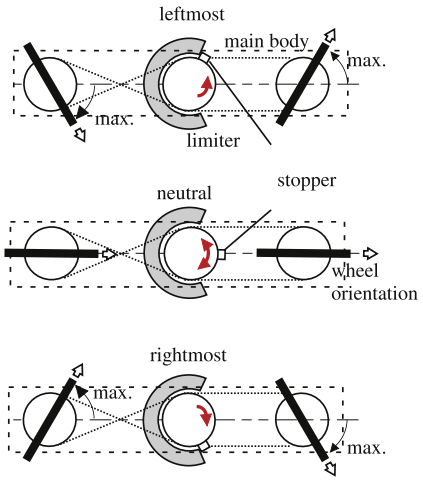

(b) Limiter and stopper for wheel orientation control

Fig. 3. Concept of mechanism for propulsion with single motor.

Next, let us consider the connection between the coupled wheel orientation and the rotor rotation. Of course, the motor must be connected to the rotor. After being attached to the motor support, the motor axis can be connected directly to the rotor rotation axis through a mechanical part like a coupling. Then, the motor support is usually fixed firmly to the main body. In the present study, however, we allowed the motor support to have a passive degree of freedom. As a result, the motor support can turn in the direction opposite to that of the rotor because of the reaction to the rotor rotation. We coupled the wheel orientation to this motor support rotation, as shown in Fig. 3(a).

With this mechanism, however, when the single motor drives the rotor, the wheel orientation continues to turn indefinitely. On the other hand, the rotor seldom rotates because the rotor is designed to have a large moment of inertia, thus providing the large reaction force needed to drive the board. Therefore, we restrict the rotation of the wheel orientation by installing a mechanical limiter, as shown in Fig. 3(b).

Although the limiter restricts the wheel orientation, the counter force with respect to the rotor rotation is conveyed to propel the main body. That is, the yaw moment is obtained as the reaction of the rotor rotation while keeping the wheel orientation constant. The dynamic and static requirements are satisfied. Note that the constant wheel orientation is determined mechanically by the limiter position.

The expected motion of this mechanism is shown in Fig. 4, where the rotor rotates clockwise (CW) in the right side and counterclockwise (CCW) in the left side. Unless mentioned otherwise, any mention of "torque" in this subsection refers to that torque which is applied to the rotor.

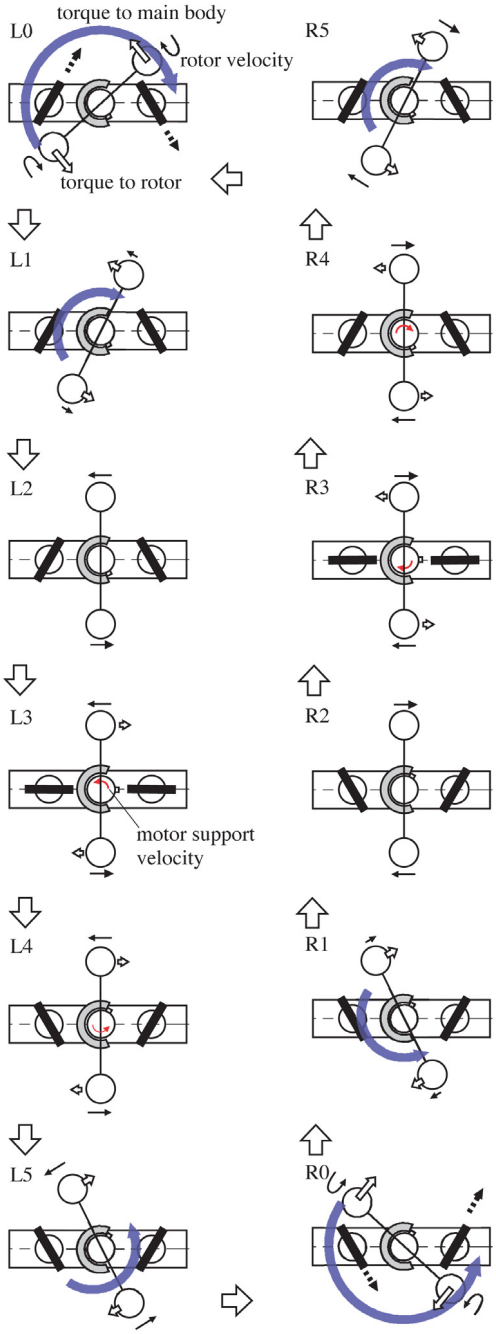

Fig. 4. Expected sequential motions.

The L0 state corresponds to the instant at which the rotor rotation reverses from CW to CCW. As can be determined by approximating the periodic rotor motion as a simple oscillation, the CCW torque becomes a maximum at this instant. Note that the motor support has already turned as far to the right as possible under the action of the CCW torque. That is, the main body is accelerated most by the counter torque through the limiter-stopper mechanism.

Although the rotor continues to accelerate in the CCW direction for a while (L1), it then begins to decelerate in the same way as in a simple oscillation. State L2 shows the instant at which the acceleration has decreased to zero.

After the L2 state, although the rotor is still rotating CCW, the torque will act in a CW direction to decelerate the rotor. In the

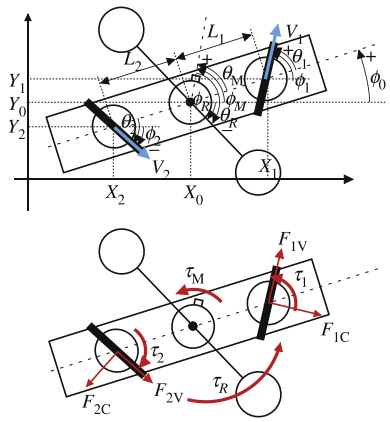

Fig. 5. Mechanical model of the board with the structure we proposed.

first instance, however, the rotor will not decelerate sufficiently. Instead, the motor support turns CCW at first (L3): This motor support rotation changes the wheel direction between the ranges defined by the limiter. The rotor is not effectively decelerated until the motor support has turned leftmost and stopped (L4).

Then, the CCW rotor rotation is gradually decelerated (L5), the rotor finally reverses (R0), and the main body is again accelerated most.

The same process happens in the opposite direction after the R0 state, and then, the state returns to L0.

3. Numerical studies

3.1. A model and assumptions

A numerical method is here introduced to investigate whether the mechanical structure in the previous section enables the skateboard robot to propel itself along the scenario mentioned in Fig. 4.

Fig. 5 shows a mechanical model that we utilized in the simulations. The followings are assumed in modeling.

- The robot moves within the horizontal plane.
- The robot is symmetrical to the front-rear, as well as the left–right, directions.
- The rotation axis of the wheel orientation is vertical.
- The robot never turns over to the lateral direction even without the side supports.
- The wheels do not slip in the axle direction.
- Viscous frictions work in the rotations as well as the robot progression.
- No decay exists in the force transmission in all the coupling.
- The collision of the stopper to the mechanical limiter is expressed by the high stiffness spring with damper.

Note that the sole input for this model is the torque for the rotor rotations.

3.2. Motion equation of the body with velocity constraints

Let Q the state vector of the skateboard robot consisting the position in the 2D horizontal space, (X_0, Y_0), and the body orientation from the X axis, ϕ_0 as

$$\mathrm{Q} = \begin{bmatrix} X_0 & Y_0 & \phi_0 \end{bmatrix}^T \tag{1}$$

The sole input for the robot is the counter moment against rotor rotation $-\tau_0$.

The robot movement is subject to the velocity constraints due to the wheels on the mid-line of the body. The wheel positions are denoted as (X_1, Y_1) and (X_2, Y_2), which are calculated from the states:

$$X_1 = X_0 + L_1 \cos\phi_0 \tag{2}$$

$$Y_1 = Y_0 + L_1 \sin\phi_0 \tag{3}$$

$$X_2 = X_0 - L_2 \cos\phi_0 \tag{4}$$

$$Y_2 = Y_0 - L_2 \sin\phi_0 \tag{5}$$

Here, the subscript distinguishes the front and rear wheels, L_1 and L_2 is the distance from the body center to each wheel. Then, the velocity of the each wheel direct exactly to the wheel orientation, ϕ_1 and ϕ_2. This fact enable us to calculate the speed of the wheel, V_1 and V_2, as follows:

$$\begin{bmatrix} V_1 \\ V_2 \end{bmatrix} = \begin{bmatrix} \dot{X}_1 \cos\phi_1 + \dot{Y}_1 \sin\phi_1 \\ \dot{X}_2 \cos\phi_2 + \dot{Y}_2 \sin\phi_2 \end{bmatrix} \tag{6}$$

Substituting the derivatives of (2)–(5) to the above relation, $\mathrm{V} = [V_1 \quad V_2]^T$ is described as

$$\mathrm{V} = \mathrm{J}_V \dot{\mathrm{Q}} \tag{7}$$

where

$$\mathrm{J}_V = \begin{bmatrix} \cos\phi_1 & \sin\phi_1 & L_1 \sin(\phi_1 - \phi_0) \\ \cos\phi_2 & \sin\phi_2 & -L_2 \sin(\phi_2 - \phi_0) \end{bmatrix} \tag{8}$$

The above fact also implies that the speed to the orthogonal direction of the wheel orientation, $V_1^\perp$ and $V_2^\perp$, which is given as,

$$\begin{bmatrix} V_1^\perp \\ V_2^\perp \end{bmatrix} = \begin{bmatrix} \dot{X}_1 \sin\phi_1 - \dot{Y}_1 \cos\phi_1 \\ \dot{X}_2 \sin\phi_2 - \dot{Y}_2 \cos\phi_2 \end{bmatrix} \tag{9}$$

are zeros. Using the derivative of (2)–(5), this relation is described as

$$\mathrm{J}_C \dot{\mathrm{Q}} = 0 \tag{10}$$

where

$$\mathrm{J}_C = \begin{bmatrix} \sin\phi_1 & -\cos\phi_1 & -L_1 \cos(\phi_1 - \phi_0) \\ \sin\phi_2 & -\cos\phi_2 & L_2 \cos(\phi_2 - \phi_0) \end{bmatrix} \tag{11}$$

The relation (10) becomes the velocity constraint of the robot.

Under this velocity constraint, the motion of the robot is represented as the following motion equation.

$$\mathrm{M}\ddot{\mathrm{Q}} = \mathrm{J}_C^T \mathrm{F}_C + \mathrm{J}_V^T \mathrm{F}_V + \mathrm{J}_U \mathrm{U} \tag{12}$$

Here, M is the inertial matrix whose components are given by the mass of the robot M including the rotor mass M_R, and the moment of inertial around the body center, I_0,

$$\mathrm{M} = \begin{bmatrix} M & 0 & 0 \\ 0 & M & 0 \\ 0 & 0 & I_0 \end{bmatrix} \tag{13}$$

F_C is the vector consisting of the constraint force satisfying (10), i.e.,

$$\mathrm{F}_C = \begin{bmatrix} F_{1C} & F_{2C} \end{bmatrix}^T \tag{14}$$

U is the moment applied to the body, and given as

$$U = -\tau_0 + \xi_Z \dot{\theta}_M - b_0 \dot{\phi}_0 \tag{15}$$

where τ_0, ξ_M and θ_M will be explained later, and b_0 is the viscous coefficient for body rotation. J_U becomes

$$J_U = \begin{bmatrix} 0 & 0 & 1 \end{bmatrix} \tag{16}$$

F_V is a vector consisting of the damping force by the frictions, i.e.,

$$F_V = \begin{bmatrix} F_{1V} & F_{2V} \end{bmatrix}^T \tag{17}$$

Here, we only consider the viscous force. Then, F_V is described as

$$F_V = -BV = -BJ_V\dot{Q} \tag{18}$$

where B is the viscous matrix:

$$B = \begin{bmatrix} b_1 & 0 \\ 0 & b_2 \end{bmatrix} \tag{19}$$

b_1 and b_2 are the viscous coefficients corresponding to each wheel.

3.3. Dynamics of rotor and wheel orientations

The motion of the rotor, the motor support and the wheel orientation can be simply represented as the dynamics of the rotating object within the 2D plane:

$$I_R\ddot{\theta}_R = -\xi_R\dot{\theta}_R + \tau_R \tag{20}$$

$$I_M\ddot{\theta}_M = -\xi_M\dot{\theta}_M + \tau_M \tag{21}$$

$$I_1\ddot{\theta}_1 = -\xi_1\dot{\theta}_1 + \tau_1 \tag{22}$$

$$I_2\ddot{\theta}_2 = -\xi_2\dot{\theta}_2 - \tau_2 \tag{23}$$

Here θ_R, θ_M, θ_1 and θ_2 denote the rotation angle of the rotor, that of the motor support, and the orientation of each wheel, respectively, with respect to the body. Namely,

$$\theta_R = \phi_R - \phi_M \tag{24}$$

$$\theta_M = \phi_M - \phi_0 \tag{25}$$

$$\theta_1 = \phi_1 - \phi_0 \tag{26}$$

$$\theta_2 = \phi_2 - \phi_0 \tag{27}$$

where ϕ_R and ϕ_M is the angular deviation of the rotor and the motor support from the positive direction of the X axis. I_R, I_M, I_1 and I_2 are the moment of inertia, and ξ_R, ξ_M, ξ_1 and ξ_2 are the viscous friction coefficients, respectively, for the rotor, the motor supporter and each wheel orientation. τ_R, τ_M, τ_1 and τ_2 are the generalized moment for them.

3.4. Coupling and limiter

This paper proposed a novel structure on which the motion of the motor support and the wheel orientation are coupled. This coupling is represented, in the basis of the rotation velocity of the motor support, as

$$\dot{\theta}_M = \dot{\theta}_1/\gamma_1 = \dot{\theta}_2/\gamma_2 \tag{28}$$

Here, γ_1 and γ_2 correspond to the reduction ratio of the motor support with respect to each wheel orientation.

The sole motor on the board, whose torque is τ, drives the rotor. Namely,

$$\tau_R = \tau \tag{29}$$

This counter force $-\tau$ rotates this coupled mechanism, i.e., the motor support as well as the wheel orientations at the same time.

The rotation of this coupling is, however, restricted by the limiters. The constraint force the limiter generates is denoted here by τ_L. Then, the practical force driving the coupling is given by the difference between the counter force of the rotor rotation and this constraint force:

$$\tau_M + \tau_1 + \tau_2 = -(\tau - \tau_L) \tag{30}$$

Consequently, the coupled dynamics are obtained by adding (21), (22) and (23) under the relation (28) and (30) as follows:

$$I_Z\ddot{\theta}_M = -\xi_Z\dot{\theta}_M + \tau_L - \tau \tag{31}$$

where

$$I_Z = I_M + \gamma_1 I_1 + \gamma_2 I_2 \tag{32}$$

$$\xi_Z = \xi_M + \gamma_1\xi_1 + \gamma_2\xi_2 \tag{33}$$

Finally, the counter force of the limiter actually propels the board itself. This means

$$-\tau_0 = -\tau_L \tag{34}$$

3.5. The force from mechanical limiter

The force, more preciously, the constraint torque from the mechanical limiter, τ_L, is here modeled as if the limiter works as the high stiffness spring with high viscous damper. Note here that the limiters are attached with the idle space for the motor support rotations. Thus, it will be represented as follows:

$$\tau_L = \begin{cases} -b_s\dot{\theta}_M + k_s(\theta_{L+} - \theta_M) & (\theta_M > \theta_{L+}) \\ 0 & (\theta_{L-} < \theta_M < \theta_{L+}) \\ -b_s\dot{\theta}_M + k_s(\theta_{L-} - \theta_M) & (\theta_M < \theta_{L-}) \end{cases} \tag{35}$$

where θ_{L-} and θ_{L+} defines the idle space of the motor support rotations, b_s and k_s are the viscous and stiffness of the limiters. Note that θ_{L-} and θ_{L+} are normally designed to be equal, and then define the maximal wheel orientation α. Actually, the relation

$$\theta_{L\pm} = \pm\alpha/\gamma_i (i = 1, 2) \tag{36}$$

holds.

3.6. Control

The robot is set to the origin $(X, Y) = (0, 0)$ with facing to the X direction, $\phi_0 = 0$, at $t = 0$. To drive the robot, the angle of the sole motor, which is equal to the rotor deviation θ_R, is controlled in order to follow the sinusoidal desired angle θ_{Rd}:

$$\theta_{Rd} = A\sin 2\pi ft \tag{37}$$

The PD control to this desired angle is applied in the simulation.

$$\tau = -K_d\dot{\theta}_R + K_p(\theta_{Rd} - \theta_R) \tag{38}$$

3.7. Simulation on propulsion

In the simulation, the parameters in the controller are set as $A = \pi/2, f = 1, K_d = 0.75, K_p = 10$. The other parameters are set as follows: $M = 3.2$, $M_R = 1.0$, $I_0 = 0.02$, $I_1 = I_2 = 0.002$, $I_M = 0.004$, $I_R = 0.015$, $L_1 = L_2 = 0.15$, $\gamma_1 = \gamma_2 = 1$, $\xi_0 = \xi_1 = \xi_2 = \xi_M = \xi_R = 0$, $b_0 = 0.01$, $b_1 = b_2 = 5$, $b_s = 7$,

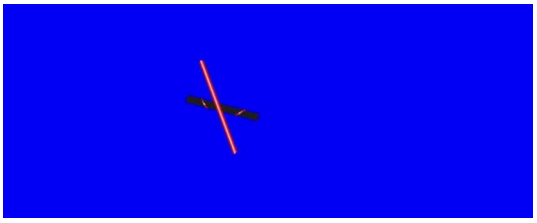

(a) A frame of animation.

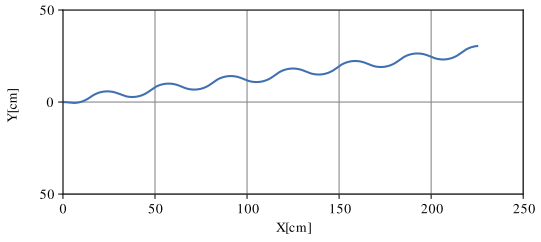

(b) The orbit on the X-Y plane.

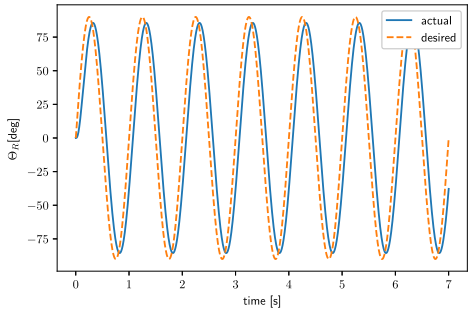

(c) The motor angle and its desired trajectory.

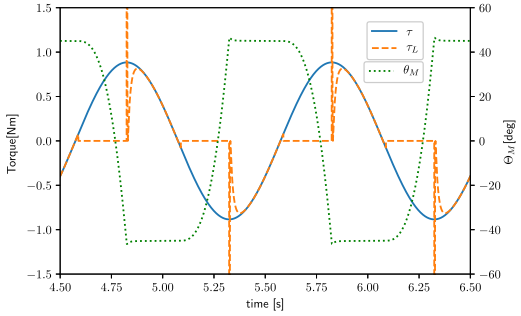

(d) Motor torque τ, torque from mechanical limiter τ_L and motor-support deviation θ_M.

Fig. 6. Simulation results.

$k_s = 500$ and $\alpha = \pi/4$. Execution time is 7 s, and the solutions are computed by the step size 0.1 ms using python 3.6.

Simulation results are depicted in Fig. 6. Fig. 6(a) is one frame of the simulated animation with OpenGL in which the robot travels rightward. The orbit of the robot during the simulated 7 s is illustrated in Fig. 6(b). We can see the robot is going straight though it is not exactly parallel to the X axis due to the effect of the transient. The time course of the rotor angle θ_R is depicted in Fig. 6(c) with its desired trajectory given as (37). Although the time delay is observed, the rotor achieves the sinusoidal swings with respect to the motor.

Fig. 6(d) shows the time course of the motor output τ, the constraint force of the mechanical limiter τ_L and the deviation of the motor support θ_M. As expected from Fig. 6(c), the torque of the single motor (the solid line) is sinusoidal. On the other hand, the limiter force (the dashed line) repeats zeros and non-zeros periodically. In the zero periods, the motor support (the dot line) rotates. Then the motor support hits the limiter, which results in the impulsive limiter force though it goes beyond the drawing range of the graph. After that, the angle of the motor support is kept at 45 deg ($\theta_{L\pm} = \pm\pi/4$) until the motor torque changes its direction. During this period, the τ_L is almost equal to τ, implying that the reaction force of the rotor rotation is surely conveyed to the propulsion force for the robot.

3.8. Effect of parameter variations

The rotor design is supposed to be crucial since this robot gains the propulsion force. The parameters about not only rotor's mass M_R and moment of inertia I_R, but also the coupling ratio γ_1 and γ_2 between the rotor (the motor support) and the orientation of the wheels, are scaled from 0.5 to 2.0 against their original value in Section 3.7. Keeping all the other parameters, the traveling distance was evaluated for 10 s simulation. The results shown in Fig. 7(a) indicates that the rotor mass and the coupling ratio have no effects to the traveling distance. On the other hand, the moment of inertia affects largely. However, this change is not monotonically increasing. Investigating this reason, the robot orbits when the moment of inertia is scaled to, 1.0, 2.5 and 4.0 are depicted in Fig. 7(b). Actually, the increment of the rotor's moment of inertia prolongs the traveling distance during one stroke of the rotor, as shown in the graph $I_R \times 2.5$. However, the moment of inertia is too large, the robot turns backward due to the large one-stroke motion as well as the large orbit curvature, as shown in the graph $I_R \times 4.0$. In that case, the rotor should turn back earlier to make the most use of the effect of inertial moment increment.

The wheel orientation θ_1 and θ_2 in the simulations are kept at the angle $+\alpha$ and $-\alpha$ during the period where the stopper-limiter mechanism is working. Thus, α is another important parameter and next we changed it in the simulation from 15 deg. to 70 deg. with keeping all the other parameters. The result is shown in Fig. 7(c). There is the optimal α as we expected. However, the optimal α was not our predicted value, 45 deg. The small α gains the traveling distance because of the small curvature of the robot orbit, but less effectively obtains the counter moment from the rotor. On the contrary, the large α facilitates the rotation, but does not enlarge the traveling distance due to the large undulation. As a result, $\alpha = 55$ deg. was the best value in this parameter set, where the rotated distance and curvature are balanced.

These numerical analyses imply that the amount of the body rotation on the undulating body orbit, that depends on the body viscous coefficient and the rotor inertial moment, has to be evaluated to the total design.

3.9. Description of our robot behaviors

To confirm that our mathematical model may describe the real robot behaviors, we attempted to replay its curved progressions, as will be shown in Section 5.4. The desired rotor motion was set as (41) by adding the increasing/decreasing offset, as the same as the experiment later. f was set to 1.2 Hz, and only the $A = 40°$ was tested with changing B from 0 to 150 in steps of 50. The 5-s duration of the simulation was also the same as experiments. The other parameters were as follows: $M = 3.2$, $M_R = 1.0$, $I_0 = 0.02$, $I_1 = I_2 = 0.002$, $I_M = 0.004$, $I_R = 0.015$, $L_1 = L_2 = 0.15$, $\gamma_1 = \gamma_2 = 2$, $\xi_0 = 0.05$, $\xi_1 = \xi_2 = 0.02$, $\xi_M = 0.04$, $\xi_R = 0.06$, $b_0 = 0.05$, $b_1 = b_2 = 2$, $b_s = 7$, $k_s = 500$ and $\alpha = \pi/6$.

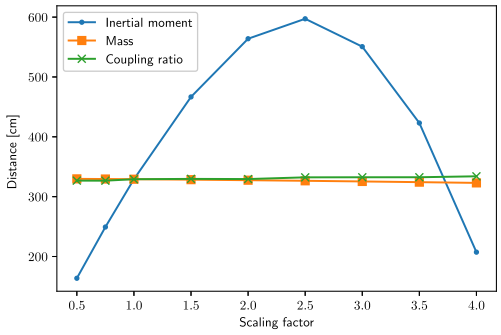

(a) Traveling distance v.s. parameter scaling

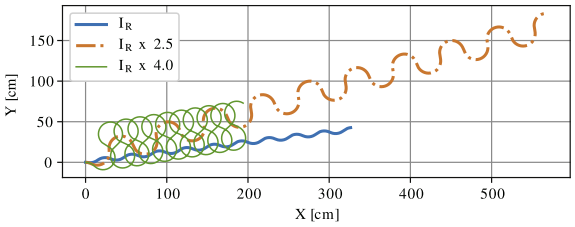

(b) Trajectories when the inertial moment of the rotor changes.

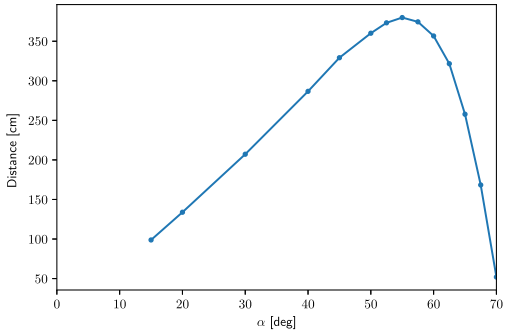

(c) Traveling distance v.s. the maximal wheel orientation α.

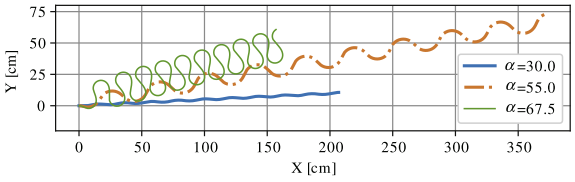

(d) Trajectories when the maximal wheel orientation α changes.

Fig. 7. Simulations under the parameter variations.

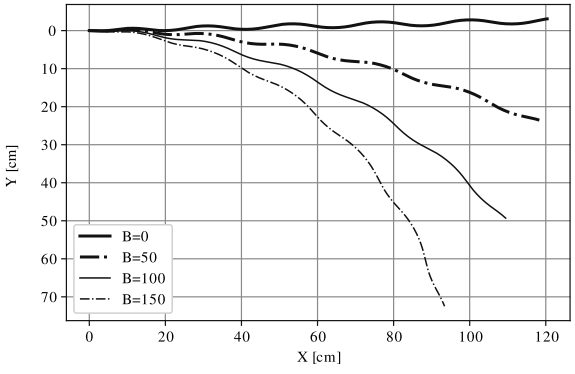

Fig. 8. Simulated curve motions reproducing Fig. 14.

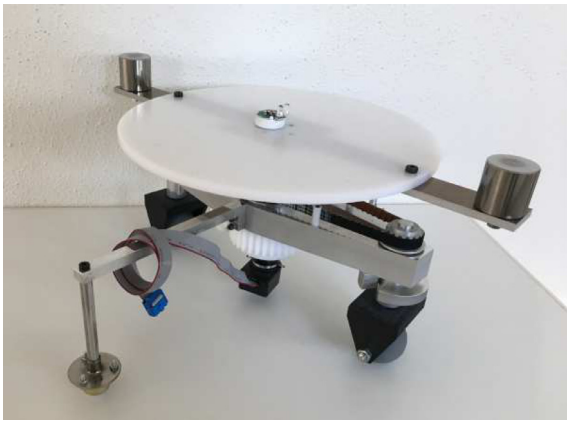

Fig. 9. Fabricated robot.

The results were depicted in Fig. 8. This reproduce the experimental results in Fig. 14 in not only the distance but also the traveling direction.

4. Robot design

This section describes how we realized our concept as a mechanical system, i.e., as a robot. The designed robot is shown in Fig. 9. It is 380 mm in length, 370 mm in width, and 183 mm in height, and weighs 3.3 kg.

The robot uses only one motor (Maxon RE25, 20 W). This motor weighs 0.29 kg, including a 128:1 reduction gear, and constitutes 9% of the total weight of the robot, pointing to the effect of the single-motor actuation on weight saving. A rotary encoder is used to detect the deviation of the motor angle.

Fig. 10 shows the drawings produced by CAD (SOLIDWORKS) at the design stage. The motor is attached to the motor support and then connected to the rotor through a coupling. The rotor consists of a shaft made of duralumin (A2017), 380 mm in length, to the ends of which carbon steel (S45C) weights are attached to increase the moment of inertia. The total weight of this is 0.9 kg, and the moment of inertia, as calculated by CAD, is 0.0155 kg m^2. A table for conveying small payloads can be attached to the rotor.

The motor support is fitted into a thrust bearing in the main body, allowing it to rotate together with the motor itself. That is, the motor support rotation is coupled to the rotation of the wheel orientation. The front wheel is simply coupled by a timing belt between pulley 1, the motor support, and pulley 2 on the wheel side, which rotates the front wheel in the same direction as the motor support. On the other hand, the rear wheel is coupled via gears and a timing belt to cause the front wheel to rotate in the opposite direction. Pulleys 2, 3, and 4, as well as gear 2, all have the same radius, as do pulley 1 and gear 1, making the orientation deviation the same for the front and rear wheels. To change the wheel orientation more quickly, a larger radius was selected for the motor support side: the ratio is 2:1.

A vertical rotation axis was introduced to support the total weight and to reduce the moment of inertia for the rotation of the wheel orientation. Therefore, sphere-shaped wheels were selected to make point contact with the floor, with the rotation axis passing through the center of the wheel. These wheel axes are attached to the main body by a bearing. Polyurethane wheels were selected to provide sufficient friction to prevent slipping.

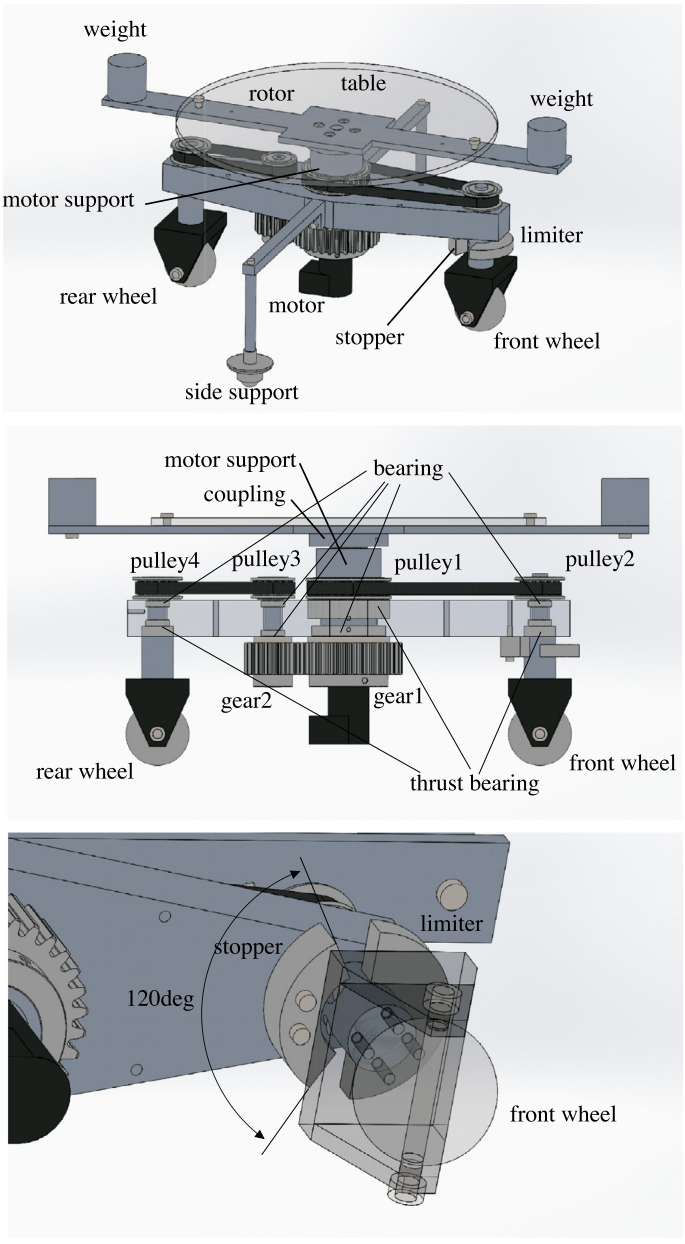

Fig. 10. Drawings produced by CAD.

The stopper and limiter were set around the rotation axis of the front wheel orientation because there is very little room around the motor support. As shown in Fig. 10, the limiter is fastened to the main body, and the semicircular stopper can move with the rotation of the wheel orientation. The angle of the limiter is set to 120°, which restricts the range of the wheel orientation to ±30°.

Safety wheels were added to provide support on both sides because the two-wheeled main body could turn over laterally without them. Omni-directional wheels were adopted to prevent these supports from impeding the smooth motion of the body.

Duralumin (A2017) was again selected to fabricate the main body. The moment of inertia around the rotor axis was 0.0305 kg m^2 on the body side.

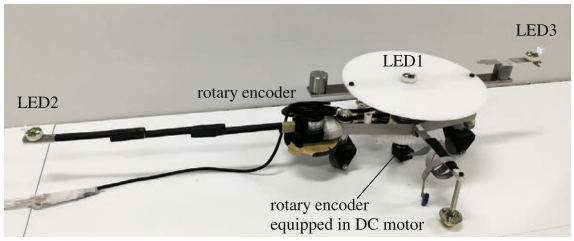

Fig. 11. Marker position for the motion capture system.

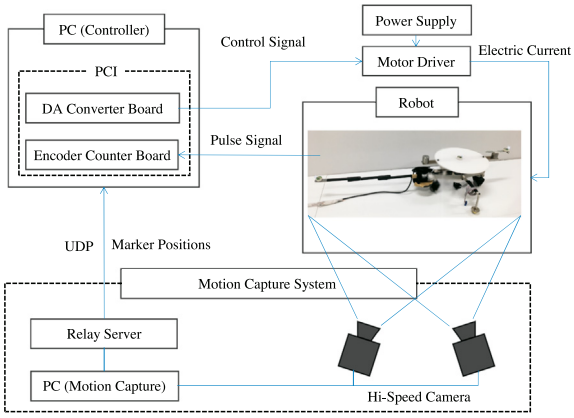

Fig. 12. Experimental setup.

5. Experiment

5.1. Objectives

This section reports the experiments that were conducted using the robot constructed as described in the previous section. The objectives of the experiments were to confirm the following:

- whether the mechanism proposed in this paper can actually propel the robot, even with only a single actuator, as expected,
- whether the asymmetrical movement of the rotor would cause the robot to progress along a curved course in a reproducible fashion,
- whether there are any relationships between the distance traveled by the robot and the amplitude/frequency of the sinusoidal rotor movement, and
- whether the feedback of positional information would allow the robot to move to the goal position.

These objectives are investigated in each sections below.

5.2. Experimental setup

A personal computer running ART-Linux was used as the controller for the robot. The output from the rotary encoder incorporated into the DC motor of the robot was connected to an encoder board (Interface PCI-6201) installed in this computer. To detect the wheel orientation, another encoder (Autonics E40HB), attached to the rotation axis of the rear wheel, was also connected to this board.

The torque computed by this computer was converted to an analog control signal for the motor driver (TITech Robot Driver PC-0121-1) using an DA converter board (Interface PCI-3120) in the computer. The motor driver output drives the robot's motor using the external power supply.

In addition, to measure the robot position in the workspace, a motion capture system (Library Radish) was introduced. This motion capture system features two high-speed cameras (Library GE60) operating at 50 Hz, and the measured positions of the markers were sent to the controller by means of UDP communication via a relay server. Three LEDs were attached to the robot center (the center of the rotor rotation), the tip of the tail extending from the main body, and one of the rotor tips, as shown in Fig. 11.

The controller operated at 1000 Hz, and for safety, the output torque was restricted to no more than ±4.97 Nm by the control program. For the control, the position control

$$\tau = K(Q_d - Q) \tag{39}$$

is adopted, where τ is the motor torque, Q is the motor (rotor) angle, and Q_d is its desired position. K is the position gain, and it was set to 0.2 throughout the experiments.

The overall experimental setup is summarized in Fig. 12.

5.3. Propulsion

5.3.1. Conditions

We simulated the robot making forward progress as a result of the sinusoidal rotor motion [21]. Thus, the desired sinusoidal position change is given to the position controller:

$$Q_d = A \sin 2\pi ft \tag{40}$$

In the experiment, we set $A = 40°$ and $f = 1.2$ Hz. The 7-s trials were conducted five times, starting from the same initial conditions in each case.

5.3.2. Results

The orbits of the robot center relative to the start position are shown in Fig. 13(a). The robot was able to propel itself even though a fluctuation in the forward direction was observed during the trials.

Fig. 13(b) shows the time course of the motor angle Q and its desired position Q_d. The rotor angle is mostly maintained at the desired position, although some delay is observed.

Fig. 13(c) shows the time course of the rear wheel orientation and motor torque τ. The almost square-shaped graph of the rear wheel orientation indicates that the wheel orientations alternate between $-30°$ and $30°$, as expected. The change in the wheel orientation starts when the direction of the rotor torque changes. After the wheel orientation has flipped, the torque value becomes a maximum. That is, the counter torque effectively propels the main body while maintaining the wheel orientations.

5.4. Curved progression

5.4.1. Conditions

The experiments described in the previous subsection indicated that symmetrical rotor oscillation produces undulating straight progress. This fact led us to assume that the robot would follow a curved path if the rotor oscillation were to be other than symmetrical, e.g., by adding an increasing offset to the sinusoidal waveform. Such an input actually causes the gradual rotation of the rotor, which must lead to rotation of the main body orientation as its counter action.

On the basis of this concept, we set the desired angle for the position control to

$$Q_d = \pm(A \sin 2\pi ft + Bt) \tag{41}$$

where B denotes the change rate of the offset.

For the experiments, we again set $A = 40°$ and $f = 1.2$ Hz by changing B from 0 to 150 in steps of 50. The 5-s experiment was conducted once for both plus and minus direction.

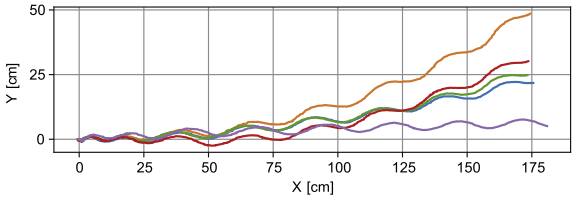

(a) Robot center orbits for each of five trials

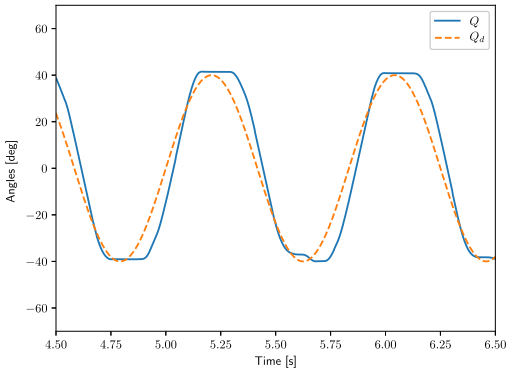

(b) Rotor angle and desired position during one experiment

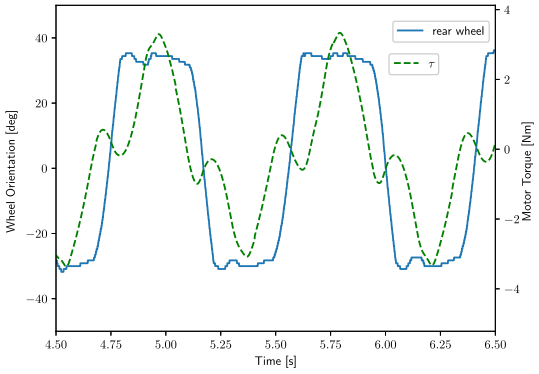

(c) Motor torque and rear wheel orientation during one experiment

Fig. 13. Results of the propulsion experiment.

5.4.2. Results

The orbits of the robot center relative to the start position are depicted in Fig. 14. The robot curves to the left when $B < 0$ or to the right when $B > 0$. The curve becomes sharper as the distance between B and 0 increases.

This experiment demonstrates that this robot can propel itself and also control the direction in which it moves by adjusting the offset change rate of the sinusoidal input.

5.5. Effect of variation in sinusoidal rotor motion

5.5.1. Conditions

All of the above experiments were performed with a constant amplitude and frequency of the sinusoidal input component. However, other combinations may propel the robot farther. This section describes how we set out to determine a better combination of amplitude/frequency in the sinusoidal input (no offset).

We adopted (40) as the desired position and changed A from $30°$ to $90°$ in steps of $10°$ for $f = 0.8$, 1.0, and 1.2 Hz. For each

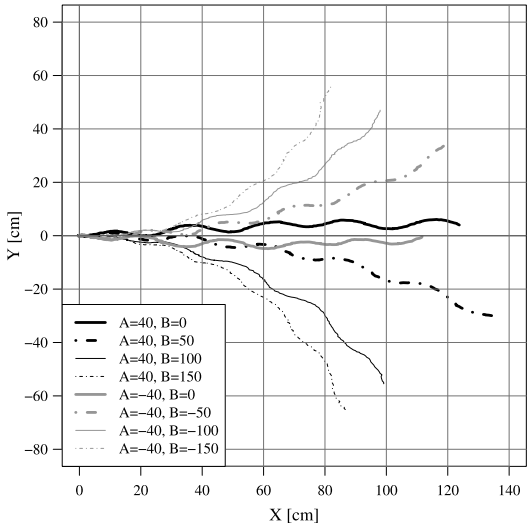

Fig. 14. Changes in robot center orbits by increasing the offset in sinusoidal rotor motion.

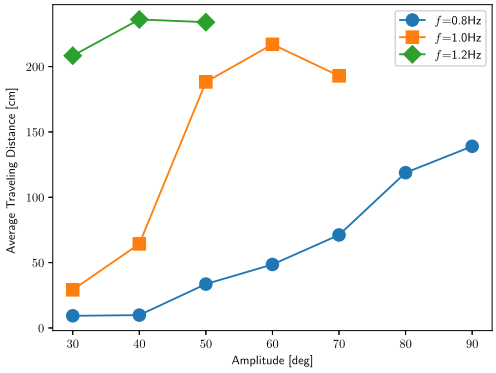

Fig. 15. Changes in traveling distance by adjusting the amplitude/frequency of sinusoidal rotor motion.

condition, an 8-s experiment was performed three times, and the average distance of travel for the three trials was used to evaluate the results.

5.5.2. Results

The experimental results are summarized in Fig. 15. The data for $A \geq 60°$ at $f = 1.2$ Hz, as well as $A \geq 80°$ at $f = 1.0$ Hz, have been removed since the torque exceeded the limit imposed for the experiment.

In each of the graphs, the distance of travel tends to increase with the amplitude: it certainly decreases at $A = 50°$ at $f = 1.2$ Hz and $A = 70°$ at $f = 1.0$ Hz. In our observations, the wheels appear to slip under these conditions. Regarding the frequency, the larger one propels the robot farther for the same amplitude. Accordingly, we can say that the larger amplitude and frequency cause the robot to travel farther, but the torque limitation and wheel slip prevent the distance from increasing monotonically. This would be reasonable since the force and acceleration monotonically increase with the amplitude and frequency if the rotor motion is assumed to be a simple harmonic oscillation. To increase the distance of travel, the largest values at which the wheels do not slip within the limits of the motor performance should be selected.

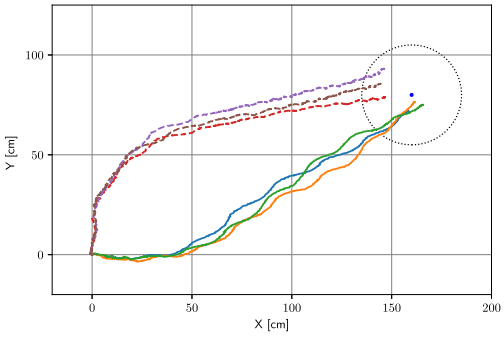

Fig. 16. Orbits of the robot center moving toward the goal position (black circle).

5.6. Controlling the motion to reach a goal position

5.6.1. Purpose

Riders of skateboards can bring themselves to a goal position by manipulating the board. We considered whether such maneuvering to a goal position would be possible by adjusting the rotor motion. Human riders usually steer the board while constantly monitoring their own position relative to the goal. Therefore, to this end, we decided to introduce positional feedback to monitor the progress to the goal position.

5.6.2. Conditions

The mission was defined as reaching the goal and stopping within 25 cm of it, regardless of the approach direction. We assumed that the goal was sufficiently far from the start position and that there were no obstacles on the horizontal floor. Then, the mission would be achieved if the board were to always adjust its direction of travel to face to the goal and then go straight toward the goal. In our experiment, we adopted this strategy to make the robot reach the goal.

The experiment described in Section 5.4 demonstrated that the change ratio of the offset to the sinusoidal rotor motion can vary the degree of the curving movement. Therefore, at the desired rotor position (41) for the control law (39), we define the adjustment rule of the offset change ratio B, such that it increases or decreases with the goal orientation ϕ.

$$B = -K_\phi \phi \tag{42}$$

where K_ϕ is the feedback gain. When the goal is immediately in front, i.e., $\phi = 0$, the offset never changes, and thus, the robot will go straight to the goal. On the other hand, if the goal is to the left, i.e., $\phi > 0$, then the offset will decrease owing to the negative B, and finally, the robot will turn to the left to orient itself with the goal, as shown in Fig. 14.

The experiment was started by placing the robot at the origin in the experimental space and then by setting the goal position to (160 cm, 80 cm). Two types of robot orientation, that is, facing the X axis and facing the Y axis, were each tested three times. K_ϕ was set to 5.

In the actual experiments, the robot propelled itself by laterally undulating, implying that ϕ always fluctuates. This fluctuating ϕ causes B to change frequently and causes the robot to undulate more. Fortunately, however, the frequency of the ϕ fluctuation is known in advance since this is caused by the rotation of the rotor at a frequency f. Thus, before adjusting B by applying (42), we applied a notch filter to remove this frequency component.

5.6.3. Results

The orbits of the robot center in these experiments are illustrated in Fig. 16. As shown here, the robot can reach the area within 25 cm of the goal position successfully even if the initial orientation of the robot is different.

6. Conclusion

This paper has addressed the single-motor propulsion of a passive-wheeled system. By applying the propulsion principle of a two-wheeled skateboard or "snakeboard", a mobile robot with a rotor and two passive spherical-shaped wheels, one in the front and one in the rear, the orientation of which was adjustable, was constructed. The novelty of the mechanism was that the sole motor driving the rotor is fastened to the main body with some free play that leads to some deviations of the motor itself as a result of the counter force to the rotor rotation. This deviation caused by the counter force is utilized to change the orientation of the wheels in the front and the rear simultaneously. The mechanism will provide a way to a new design of the mobile robot from not only the point that the number of the required motor is only one, but also that the wheels are still passive: we can easily push and pull this, without disconnecting the clutch, unlike the active wheel system. It will be applicable to, e.g., shopping cart: a user takes it along freely, but in need it can autonomously move.

The propulsion based on the mechanism was confirmed with numerical analyses using a mechanical model. The numerical analyses also elucidated that the rotor' moment of inertia, the maximal wheel orientations, the frequency of the rotor repetitive motion and their combination should be considered to prolong the robot traveling distance.

The robot experiments confirmed that

- the mechanism proposed in this paper allows a robot to propel itself using the sinusoidal rotations of a rotor,
- the robot can turn by increasing or decreasing the offset of the sinusoidal rotor motion, and a larger acceleration of the rotor can propel the robot more effectively,
- feedback of the robot position allows the robot to progress toward a goal position, even when propelled by only a single motor.

The first experiment becomes an evidence on the working principle of the propulsion mechanism we propose. The findings in the second experiment certainly contributes to enlarge the maneuverability of this mechanism. It indicates that adjusting the changing rate of the sinusoidal offset can plan the path to the goal position. The relation between the changing rate and the path curvature might be calculated theoretically, but it will be affected from, e.g., the damping rate of the moving speed of the robot, and thus should be investigated experimentally in the actual application. The last experiment is a good demonstration to bring the snakeboard robot to the goal position, whose main discussions have been restricted mainly in the mathematical theory or the computer simulations in related studies.

All these experiments provide the facts the robot with single actuation mechanism can achieve by showing the robotic movements, though more theoretical analysis will be required more. Namely, the experimental results here contribute to a new design of the mobile robot as the experimental evidences and the indication of its future development orientation. In our future work, we will further investigate the effect of the spring to further improve the efficiency and will apply this mechanism to a power-assisted system capable of actually conveying a load.

Declaration of competing interest

The authors declare that they have no known competing financial interests or personal relationships that could have appeared to influence the work reported in this paper.

Acknowledgments

This research did not receive any specific grant from funding agencies in the public, commercial, or not-for-profit sectors.

Appendix A. Supplementary data

Supplementary material related to this article can be found online at https://doi.org/10.1016/j.robot.2019.103310.

References

[1] J. Ostrowski, J. Burdick, Controllability tests for mechanical systems with symmetries and constraints, J. Appl. Math. Comput. Sci. 7 (1997) 101–127.
[2] F. Bullo, A. Lewis, Kinematic controllability and motion planning for the snakeboard, IEEE Trans. Robot. Autom. 19 (2003) 494–498.
[3] S. Iannitti, K. Lynch, Minimum control-switch motions for the snakeboard: A case study in kinematically controllable underactuated systems, IEEE Trans. Robot. 20 (2004) 994–1006.
[4] T. Narikiyo, Control of underactuated mechanical systems via passive velocity field control: Application to snakeboard and 3D rigid body, Nonlinear Anal. 71 (2009) e2358–e2365.
[5] E. Shammas, M. De Oliveira, Motion planning for the snakeboard, Int. J. Robot. Res. 31 (2012) 872–885.
[6] T. Dear, R.L. Hatton, M. Travers, H. Choset, Snakeboard motion planning with local trajectory information, in: ASME 2013 Dynamic Systems and Control Conference, American Society of Mechanical Engineers, 2013, pp. DSCC–2013–3883.
[7] T. Dear, S.D. Kelly, M. Travers, H. Choset, Snakeboard motion planning with viscous friction and skidding, in: 2015 IEEE International Conference on Robotics and Automation (ICRA), IEEE, 2015, pp. 670–675.
[8] S. Derammelaere, C. Copot, M. Haemers, F. Verbelen, B. Vervisch, C. Ionescu, K. Stockman, Realtime locomotion control of a snakeboard robot based on a novel model, enabling better physical insights, Eur. J. Control (2018).
[9] S. Hirose, H. Yamada, Snake-like robots [tutorial], IEEE Robot. Autom. Mag. 16 (2009) 88–98.
[10] T. Takemori, M. Tanaka, F. Matsuno, Gait design for a snake robot by connecting curve segments and experimental demonstration, IEEE Trans. Robot. (2018).
[11] P. Krishnaprasad, D.P. Tsakiris, Oscillations, se (2)-snakes and motion control: A study of the roller racer, Dyn. Syst.:Int. J. 16 (2001) 347–397.
[12] H. Mori, T. Nagamine, T. Ichijo, Y. Sato, Effects of friction on driving mechanism using swing motion, Trans. JSME 81 (2015) 15–00330, (in Japanese).
[13] S. Chitta, P. Cheng, E. Frazzoli, V. Kumar, Robotrikke: A novel undulatory locomotion system, in: IEEE International Conference on Robotics and Automation, Vol. 2, Citeseer, 2005, pp. 1597–1602.
[14] G. Endo, S. Hirose, Study on roller-walker – improvement of locomotive efficiency of quadruped robots by passive wheels, Adv. Robot. 26 (2012) 969–988.
[15] M. Li, S. Guo, H. Hirata, H. Ishihara, A roller-skating/walking mode-based amphibious robot, Robot. Comput.-Integr. Manuf. 44 (2017) 17–29.
[16] S. Ito, S. Takeuchi, M. Sasaki, Motion measurement of a two-wheeled skateboard and its dynamical simulation, Appl. Math. Model. 36 (2012) 2178–2191.
[17] T. Wang, B. Su, S. Kuang, J. Wang, On kinematic mechanism of a two-wheel skateboard: The essboard, J. Mech. Robot. 5 (2013) 034503.
[18] B. Su, T. Wang, R. Wu, J. Wang, Infimum of path length of nonholonomic vehicle with finitely bounded curvature radius, J. Intell. Robot. Syst. 79 (2015) 197–210.
[19] K. Kinugasa, M. Ishikawa, Y. Sugimoto, K. Osuka, Modeling and control of casterboard robot, IFAC Proc. Vol. 46 (2013) 785–790.
[20] S. Ito, S. Sugiura, Y. Masuda, S. Kiely, J. Yabuki, R. Morita, A mechanism of single actuator snakeboard robot and its curving motion generation, in: 2018 IEEE International Conference on Robotics and Biomimetics (IEEE ROBIO 2018), 2018, pp. 1232–1237.
[21] S. Ito, S. Sugiura, Y. Masuda, S. Nohara, R. Morita, Mechanism and control of a one-actuator mobile robot incorporating a torque limiter, J. Intell. Robot. Syst. (2019) http://dx.doi.org/10.1007/s10846-019-01036-8.

Satoshi Ito received the B.E. and M.E. degrees from Nagoya University in 1991 and 1993, respectively. He worked at Bio-Mimetic Control Research Center, RIKEN as a technical staff from 1994 to 1997 and a Frontier researcher from 1997 to 1999. In 1999, he received his Dr. Eng. degree from Nagoya University. He was a research associate at the Faculty of Engineering, Gifu University in 1999, and was an associate professor in 2004. He has been a professor at Gifu University since 2015.

Kosuke Niwa received the B.S. and M.S. degrees in engineering from Gifu University, Japan, in 2016 and 2018, respectively. Currently, he works in Yamaha Motor Co., Ltd.

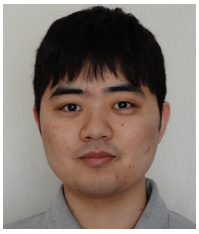

Shoya Sugiura received the B.S. degree in engineering from Gifu University, Japan, in 2018. He is currently a student of graduate school of Natural Science and Technology, Gifu University.

Ryosuke Morita received the B.S. degree in engineering, the M.S. and Ph.D. degree in informatics from Kyoto University, Kyoto, Japan in 2008, 2010, and 2013 respectively. From 2013 to 2014, he was a Specially Appointed Researcher in Graduate School of Information Science and Technology, Osaka University, Suita Japan. From 2014 to 2015, he was an Assistant Professor of the College of Science and Engineering, Aoyama Gakuin University, Sagamihara, Japan. He is currently an Assistant Professor of the Faculty of Engineering, Gifu University, Gifu, Japan.